Ice-Type Characterization in a Marginal Ice Zone Using RADARSAT and Ice-Profiling Sonar: Tools for Structural Design and Navigation Planning in Ice Infested Waters

J.R. Marko, D.B. Fissel and K. Borg

ASL Environmental Sciences Inc., Sidney, B.C., Canada

ABSTRACT

Advanced versions of moored sub-surface ULS (upward-looking sonar) instrumentation, originally developed (Melling et al., 1995) to provide high resolution mappings of ice draft in mobile pack ice have been a prominent component of recent hydrocarbon exploration and production activities in ice covered waters. In each case, data gathered by adjacent ice- and acoustic Doppler current-profilers have provided quasi-spatial profiles (QSPs) equivalent to quasi-continuous sampling of ice-draft along linear ice tracks. These products have offered a basis for generating ice draft/thickness statistics descriptive both of the overall regional ice covers as well as of individual ice features relevant to navigation and offshore structure design and protection.

The basic methodology of ice profiling is described and illustrated in terms of ASL's IPS4 Ice Profiler instrument. After a brief description of Radarsat SAR imagery and its applications to ice cover characterization, focus is given to results obtained on the continental shelf in the Sea of Okhotsk east of Sakhalin Island which allow comparisons of such imagery with near-simultaneously obtained draft profile data. Such comparisons facilitate evaluations of the capabilities of Radarsat SAR imagery to detect topographic features of the ice cover of concern to the offshore oil industry. Operational issues such as the remote detectability of exceptionally large (and deep) ice ridges are addressed and results presented on the observability of other ice-topographic categories of significant potential interest. Statistical characterizations of the identified ice-types are compared with available remote sensing data and with the history of the observed ice cover.

INTRODUCTION

The introduction, over the past decade, of high frequency range-sampling from special-purpose moored upward-looking sonar (ULS) units deployed near ice velocity-measuring sonar (Melling et al., 1995) has offered the offshore oil industry and the scientific community practical capabilities for long-term collection of undersurface topography data in mobile ice fields. Data of this type collected in Arctic Basin and Antarctic waters supplement and offer increasingly valuable alternatives to similar information previously acquired only from ULS instruments on board military submarines irregularly transiting these same regions. Consequently, related collection efforts are likely to be essential

components of future programs directed at using polar ice covers as indicators of climate change. On the other hand, profiling data gathered for the offshore-oil industry, although of considerable climatological significance (particularly, when available over extended, multi-year intervals), have been largely proprietary in nature and used to establish basic local ice draft statistics and probabilities for encountering ice objects of extremal sizes for, primarily, offshore structure and navigation design purposes. Nevertheless, in some instances, industry-sponsored acquisitions of draft data have led directly to quantitative study and characterization of unusual, operationally significant, events such as appearances of intense wave activity hundreds of km inside the boundaries of marginal ice zones (Marko, 2001, 2003).

In almost all instances, utilization of information obtained from moored ULS instruments encourages retrospective use of data accumulated over extended periods of time (i.e. over a single or multiple annual ice seasons) and recovered during seasonal clearances. Industry needs for near-realtime access to such information have, thus, encouraged use of retrospective use of ULS draft data to guide quantitative interpretation of high-availability, all-weather satellite or aircraft imagery.

The present report is based upon one such effort directed at exploring capabilities for recognizing the presence of large ice keels (the under-water portions of ice ridges) in Radarsat Synthetic Aperature Radar (SAR) image products. Sponsored jointly by the Canada Centre for Remote Sensing, the Joint Industry Program for research in the Sea of Okhotsk and its original participants, the Sakhalin Energy Investment Company Ltd. and Exxon Neftegas Ltd., these explorations were based upon analyses of Radarsat single beam images of the Sea of Okhotsk east of Sakhalin Island in conjunction with data from the same areas gathered with a regional array of moored ice profilers and accompanying current- and ice drift-measurement instruments. A fundamental objective of this work was to establish the extent to which large ice keels are detectable on radar imagery. Inevitably, in the course of this work, other, potentially operationally significant, linkages were established between the characteristics of an ice undersurface and the corresponding Radarsat signatures of its above-water counterparts.

MOORED ICE PROFILING METHODOLOGY AND DEPLOYMENTS

A typical moored ice-profiling installation is depicted in Figure 1 in the form of adjacent deployments of an ASL IPS4 *Ice Profiler* and an RDI ADCP (Acoustic Doppler Current Profiler. The *Ice Profiler* measures time delays associated with returns of its narrow beam (1.8˚) pulses of 420 kHz ultrasound. These returns are converted into ranges through use of: on-board sampled hydrostatic pressure, independent sea level atmospheric pressure data; and estimates of the speed of sound in the water column above the instrument. The latter estimates are derived from previous and subsequent (to deployment) temperature and salinity profiling at the site combined with required compatibility between the measured hydrostatic pressure values and calculated ranges associated with unambiguously recognizable patches of open, ice-free water. Time series ice velocity data from the ADCP instrumentation allows conversion of the obtained draft data into quasi-spatial profile (QSP) products such as depicted in Figure 2.

Ice Profilers deployed at a depth of about 30 m have a, roughly, 1 m diameter footprint on the ice undersurface. With only routine efforts to maximize the accuracy of sound speed recalibrations, QSP's generated from the Sea of Okhotsk data sets were, typically, capable of representing draft values at 0.5m intervals with +/- 20 cm accuracy.

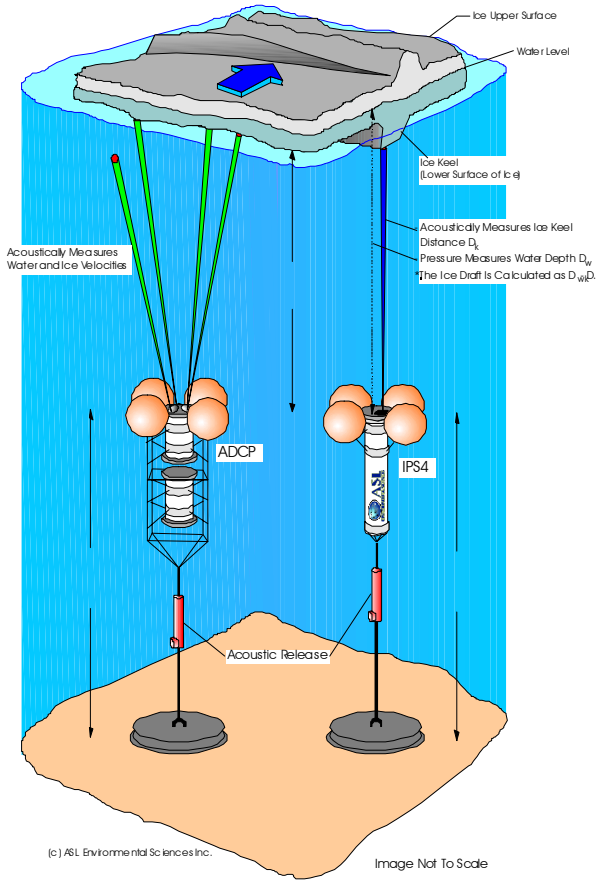

Figure 1. Schematic illustration of typical deployment of ice-profiling and ice-tracking ADCP instrumentation.

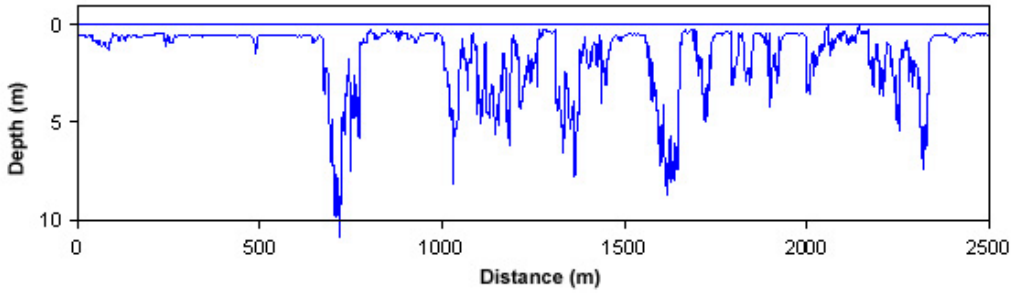

Figure 2. Quasi-Spatial Profile representation of ice draft data, gathered over the northeastern Sakhalin Island shelf, March 20, 1998.

In the 1996-997 winter JIP program, 6 IPS4 units were deployed at 6 sites on the continental shelf east of Sakhalin Island as indicated in Figure 3. Instruments at four of these sites (PA3, PA2, AD1 and AD2), deployed in waters with depths between 35 m and 60 m, were immediately adjacent (within about 100m) to moored ADCP instruments, one of which (at PA2) returned only a very incomplete data record. The remaining two sites, PA1 and Chayvo, were in shallower waters where the profiling instruments were replaced by single level, near bottom (WHISL) current meters manufactured by Woods Hole Instrument Corp. The latter instruments did not have a capability for measuring ice drift, necessitating that the ice velocities required for production of local QSPs had to be based upon local near-bottom current time series data assuming the applicability of multiple regressions of ice velocity on wind and equivalent near bottom current values as derived for the closest ADCP-equipped monitoring site. With the exception of the PA3 site, where the IPS4 instrument was lost (presumably to fishing activity), these deployments allowed successful generation of QSP draft records at all monitoring sites over the period November, 1996 to late May, 1997.

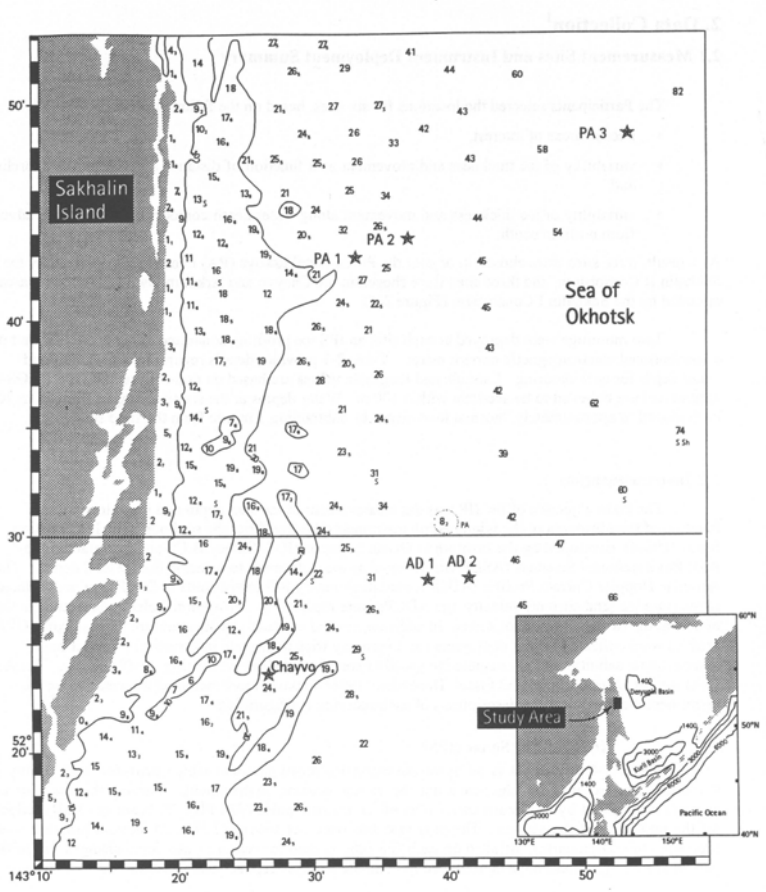

Figure 3. Site locations associated with the 1996-1997 monitoring array. The location of the study area in the greater Sea of Okhotsk region is indicated in the inset.

RADARSAT SAR IMAGERY

Eleven single beam Radarsat images were acquired for use in this study, spanning, roughly, a month-long period in late winter-early spring, 1997. Timing, coverage and

spatial resolution details are provided in Table 1 for 7 of these images. Similar data from 4 other images acquired for April 1 and 8 proved not to be of use for our study since the nearly continuous presence of moderate to strong westerly winds in the March 24- April 8 period moved all of the pack ice to the east of the pre-selected Radarsat fields of view. The last column of the Table includes the range of incidence angles (measured relative to the vertical direction) spanned in each image as a guide to assessing the expected effectiveness of detection for the deformed ice surfaces of operational interest. Expectations were (Melling, 1998) that the strength of reflected radar returns from ridged ice, although largely determined by relatively small scale geometrical details of ridge composition, should increase with a ridge's fractional occupation of the sensing beam's footprint (i.e. with the beam filling factor). Maximizing these filling factors by using oblique incidence beams tends to enhance the contrast between ridges and adjacent level ice. Unfortunately, early studies (Pearson et al., 1980) of fully beam-filling ridges at slightly higher (10GHz vs. 5.7GHz) frequencies but with identical (horizontal) transmission and reception modes showed negligible sensitivities to incidence angles between 25˚ and 55˚ which spanned the range incorporated in our test imagery. The accompanying conclusion that optimal ridged- vs flat-ice contrasts were achieved with incidence angles in the range: 70˚ to 85˚, confirmed in airborne SAR studies (Melling, 1998), suggests that essentially all Radarsat observation modes are less than ideal for ridge detection and assessment. It was our objective to assess the extent to which these shortcomings in its fundamental operational parameters limit Radarsat's usage can be overcome to allow recognition and characterization of large deformed ice masses.

Date	Time	Lat. (˚N)	Long. (˚W)	Beam Mode	Pixel Dim.(m)	Looks	Image Dim. (km, km)	Incid.Angle (˚)
Mar.22	8:15	52˚ 41'40"	143˚ 28'2"	S5	12.5	4	113,101	36-42
Apr.1	20:30	52˚ 43'35"	143˚ 26'16"	F5	6.25	1	38,49	45-48
Apr. 15	8:15	52˚ 36'0"	143˚ 318'58"	S5	12.5	4	112,101	36-42
Apr. 18	20:34	52˚ 23'20"	143˚ 27'36"	F3	6.25	1	39,50	41-44
Apr. 18	20:34	52˚ 44'0"	143˚ 33'13"	F3	6.25	1	39,50	41-44
Apr. 25	20:30	52˚ 42'59"	143˚ 26'19"	F5	6.25	1	38,50	45-48
Apr. 25	20:30	52˚ 22'8"	143˚ 21'17"	F5	6.25	1	38,50	45-48

Table 1. Basic Parameters associated with Radarsat images provided by Radarsat International for use in this study.

DRAFT/IMAGE COMPARISONS

Correspondences between notable topographic ice cover features and equivalent portions of the Radarsat images were evaluated using QSP draft vs. displacement plots and their associated statistics as obtained for ice traversing the IPS-4 monitoring sites at times spanning, roughly, 48-hour periods centred on the recording times of individual images. This evaluation followed initial efforts to classify the broader ice types in the region which could be associated with relatively robust Radarsat reflectance signatures. This work utilized standard enhancement techniques and colour-coded displays of ice draft statistics for individual segments of the curvilinear trajectories traced out by the individual IPS-4 beams on the moving ice surface. Within the limited capabilities for image navigation and specification of ice movements, the latter displays directly tested capabilities for remote recognition of surface features characterized by subsurface keel depths of known magnitudes.

A typical decimated (i.e. below full resolution) standard beam image, recorded on April 15 is displayed in Figure 4. Numerical labels denote areas with commonly observed Radarsat ice signatures of interest and open circles represent the 5 sites where IPS4, ice velocity and current data were successfully collected. The key signatures of note were: numerous areas of high brightness (Features 3, 4a, 4b) and much better defined, floe-like dark areas (Features 2a, 2b). The bright features appear both near the outer ice edge where we expect a highly reflective mixture of broken ice and waves and in the high radiance matrix of the “mottled“ zone near the western, shoreward, edge of the ice.

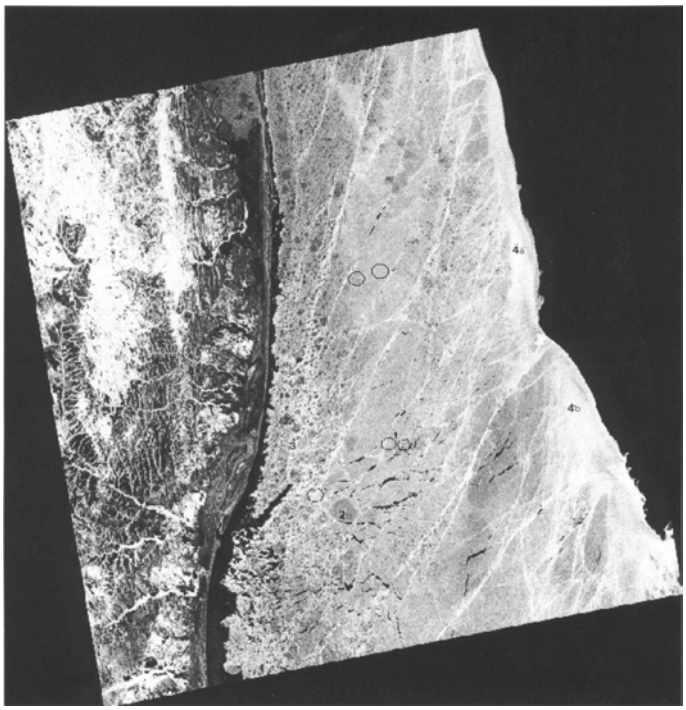

Figure 4. A decimated Standard Beam image of the study area acquired on April 15, 1997. Instrumented sies, identified in Figure 3, are denoted by open circles and numerical annotation denote locations of ice types discussed in text.

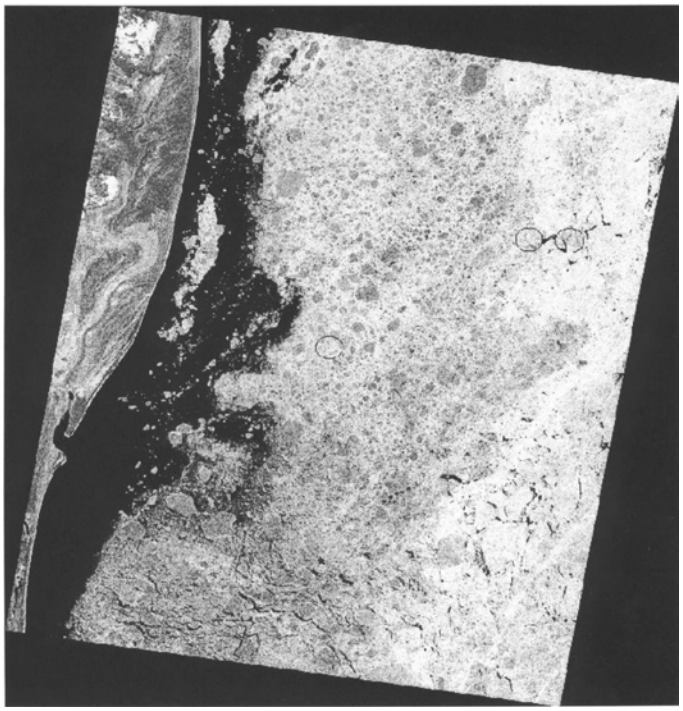

Figure 5. A decimated Fine Beam image of the southern portion of study area acquired on April 18, 1997. The positions of the three southernmost monitoring sites are denoted by open circles.

The floe-like appearance of the dark area features in the mottled zone and elsewhere is more evident in a higher resolution April 18 image (Figure 5) and is consistent with the low radar reflectivity expected of continuous floe-like areas of flat ice with diameters ranging up to several km. The third, and perhaps most interesting category of ice evident in Figure 4, denoted as Feature 1, was designated as "anomalous bright ice" because of its unique combination of highly uniform but intermediate pixel brightness. This uniformity and the considerable size of the region covered by such ice is most evident in Figure 4, while its overall elevation of brightness relative to the adjacent mottled zone is most apparent at higher resolution (Figure 5). Quantitative comparisons of the distributions of pixel values (Figure 6) relative to those of the adjacent mottled ice highlight the narrowness of the anomalous ice pixel distribution and the associated relative absence of the long high brightness tail which is characteristic of other ice types encountered in our study. These distinctions are, moreover, mirrored in the corresponding draft probability data obtained for the two ice types (Figure 7). Specifically, the mottled and other observed ice types tended to show the expected (Wadhams, 1998) exponential falloff in probability for drafts above relatively broad peaks of the distributions which tend to occur at drafts close to the regional mean values which are usually between 1 and 2 m. The anomalous bright ice, on the other hand, was characterized by a much narrower, almost Gaussian, distribution with an effectively negligible tail at high draft values and essentially no ice thinner than about 0.5 m. Additionally, comparisons of typical QSPs of this ice with its mottled ice counterpart (Figure 8) display its characteristically high roughness or point to point draft variability which is consistent with its characteristically high Radarsat radiance. The latter variability yields draft variance values which are intermediate to those associated with mottled ice and the low radiance flat floe

component of such ice. These features of the anomalous bright ice, namely extreme compactness (negligible thin ice or open water), a narrow peaking of the draft distribution somewhere above 3 m, combined with the effective absence of the high draft values associated with the presence of large ice ridge keels are of considerable operational significance particularly because of the relatively easy radar detectability of their host ice type. Thus, they allow significant portions of, at least, some ice packs to be identified as extremely unlikely habitats for the large ice ridges which can pose major hazards to offshore structures and shipping. Moreover, relevant to the present study, the coincident absence of both extremely bright Radarsat pixels and large draft values in this ice type suggests that, indeed, even at the steep Radarsat observation angles, high ridge sails, which, presumably, are roughly coincident with deep ridge keels, do contribute Radarsat signal intensities well in excess of those associated with, at least, rough and flat ice of moderate to high mean thickness.

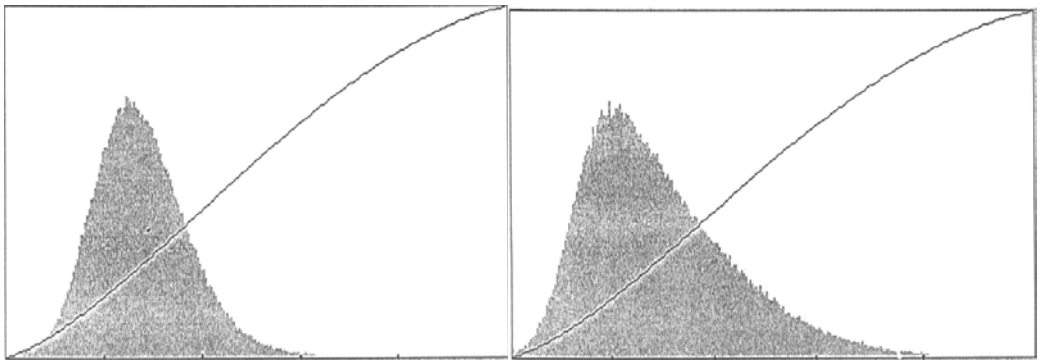

Figure 6. Probability distributions for Radarsat pixel brightness (plotted with brightness levels between 0 and 255 at the left and right hand sides, respectively, of the horizontal axis) for: a) the anomalous bright ice type; b) the mottled ice type.

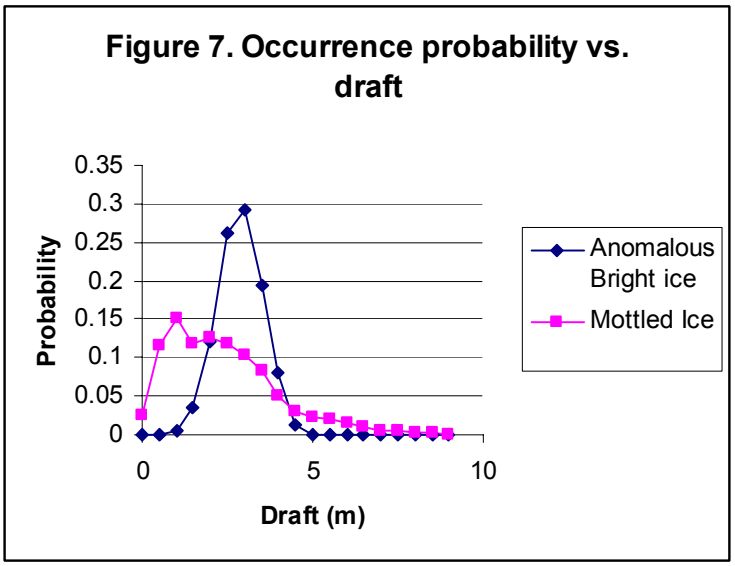

Figure 7. Typical draft probabilities as measured in the anomalous bright ice and mottled ice regions.

Given the ubiquity of the anomalous bright ice when present (it comprised more than 25 % of the observed ice covered area in the last 3 weeks of April) there is some interest in understanding its origins as an apparent consequence of the above noted, early April period of strong and sustained easterly winds. These winds closed the previously existing coastal polynya and greatly compressed the regional ice pack against the Sakhalin Island coast. Comparisons with earlier imagery and ice chart data suggest that this forcing collapsed an ice pack which extended at least 300 km outward from the coastline into a compact mass of widths as small as 5 km.

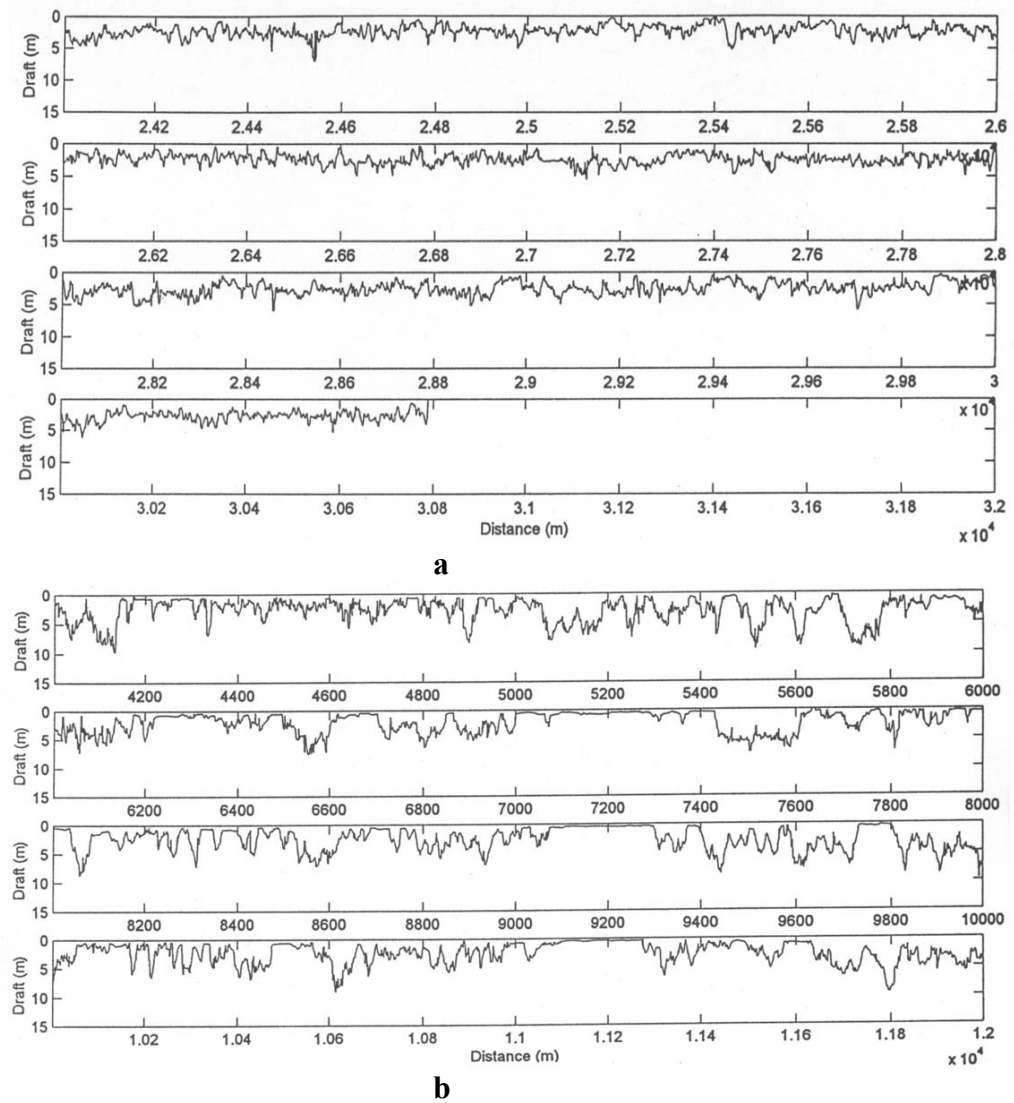

Figure 8. April 15, 1997 ice draft profiles (QSPs) for: a) anomalous bright ice (measured at AD1); b) mottled ice (measured at Chayvo).

If, indeed, the anomalous bright ice type was constructed out of the mostly thinner portions of the pack ice to seaward of a more shoreward band of thicker, less compressible ice a few tens of km in width, one might expect that the absence of keel drafts larger than about 5 m might be able to tell us something about the utilized ice

matrix from the empirical connections noted by Melling and Reidel (1996) between maximum keel draft, $h_{max,}$, and the adjacent level ice thickness, d. This relationship:

$$h_{max} = 20d^{0.5}. \qquad \text{(Eq. 1)}$$

used in conjunction with the observed an upper keel depth limit of 5 m implies that the anomalous ice in question was formed from level ice of approximately 0.16 m in thickness. Creation of the, typically 10 to 15 km wide fields of the anomalous ice type with the observed high (> 3 m) mean thicknesses would have required compression of 200 to 300 km wide portions of the outer Sakhalin ice fields. Contemporary ice chart and satellite imagery suggest that considerable fractions of the ice in the offshore ice fields prior to the compression event were associated with 30 to 120 cm ice thicknesses, allowing accumulation of > 3 m mean ice thicknesses with much less drastic ice pack compressions. In the absence of additional data, the absence of large keels can be taken either as evidence of the critical role played by the thinner ice portions of the offshore pack ice in production of the anomalous ice type or as an indication that the compressional/flexural strength of the corresponding deformed ice type is only equivalent to that of level ice a few tens of cm in thickness. A reasonable guess is that the anomalous ice form is constructed out of multiple "rafted" layers of the ice of moderate to low thickness similar to that previously photographed in the Gulf of Bothnia by Scott Polar Research Institute personnel (Figure 9). In addition to its significance to shipping and offshore structures, the mechanical properties of this ice type may also be relevant to wave activity in inshore areas, since there is indirect evidence that similar ice may have allowed large wave amplitudes to penetrate into ice of considerable thickness in areas hundreds of km inside the outer pack ice boundary (Marko, 2003).

Figure 9. A multi-layer, rafted ice field in the Gulf of Bothnia (SPRI photograph)

Although this demonstrated capability for recognizing familiar and not so familiar ice types was useful, the operational utility of Radarsat for offshore structures in ice-covered waters would still be greatly increased by demonstrated capabilities to detect large ridge-like objects usually associated with the keels of great depth and length frequently detected by our sub-surface profiling instrumentation. Our tests of such capabilities utilized various enhancements of the imagery in conjunction with colour-coded overlays of measured draft statistic parameters along the imaginary tracks traced by the fields of view of individual IPS4 monitoring instruments on the moving regional ice surface. Ice statistic parameters used in these tests were the means, maxima and standard deviations of all draft samples recorded within successive segments of lengths equal to nominal 6.25 m and 12.5 m linear dimensions of the fine and standard beam images. In practice, with regional typical mean drift velocities of 20 cm/s, this procedure incorporated 30 to 60 individual draft measurements into each draft statistic. The positions of the individual ice cover points on the trajectory were calculated using the +/-100m estimated accuracy of the Radarsat images to locate the monitoring sites on each image and then working backwards and forwards in time using the ice velocity record at each site to find the approximate positions on the images of all ice which passed over the monitoring sites during the 24 hour periods prior to and immediately following the image recording time.

Realistic comparisons between image and draft profile characteristics required allowances for the above-noted uncertainties in image navigation and in the additional positioning uncertainties built into all ice not directly over the monitoring sites at the time of image recording. The latter uncertainties arose from imperfections in our knowledge of the ice velocities used in the ice drift calculations. Assuming that errors in the assumed velocity were primarily associated with a +/- 1° directional uncertainty, the radii of the 100 m radius "error circles" surrounding the ice at each IPS4 site on each image were found to, typically, increase by 100 m for every 2 hours of additional displacement of a given draft measurement from the time of image recording. Under such circumstances, it proved essentially impossible to consider making image-draft comparisons for ice which passed over the monitoring sites at times preceding or following the image time by more than about 6 hours.

Comparisons utilized several different black and white and colour-coded image displays with it eventually being decided that the best overall correspondences were achieved with a square law display (i.e. the pixel values were scaled as the square of the recorded Radarsat radiance values). A similar display technique had previously been shown to significantly increase correlations between airborne SAR and IPS4 data (Melling, 1998). Its effectiveness in highlighting exceptionally high radiance image features is illustrated in Figures 10a,b where we have displayed linear and square law full resolution images of a mottled ice region from the March 22 image. The linear display (Figure 10a) shows a collection of "dark" flat floes with diameters ranging up to and slightly beyond 100 m embedded in a matrix of high radiance ice and almost completely black patches of open water. The square law display (Figure 10b) shows more clearly that objects of exceptional brightness, and, hence, potential large ridge candidates, are almost exclusively confined to the interstitial regions on the peripheries of the apparently flat floes. This built-in emphasis on exceptionally high radiance objects facilitated testing of

correlations with objects of exceptional draft since it was not found possible to set linear display thresholds sufficiently high to both avoid abundant appearances of bright features close to nominally thin ice and yet allow such features to be consistently present within the circle of uncertainty of known (from IPS4 data) deep draft features.

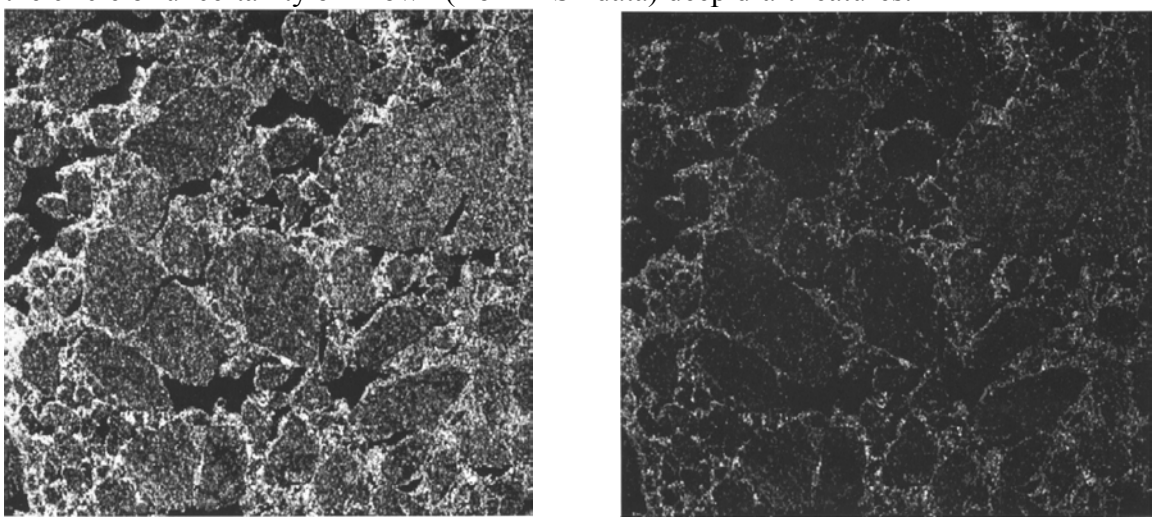

a b

Figure 10. A full resolution portion of the March 22, 1997 Standard Beam image in a region occupied by the mottled ice type as displayed using: a) a linear brightness vs. pixel value relationship; and b) a square law relationship.

The best demonstrations of correlations utilized square law displays of imagery from the mottled ice zones associated with the most diverse mixtures of ice types. As seen in the Fine Beam image of ice near Chayvo on April 18, Figure 11, overlays of maximum draft values along a given track confirm that the lowest maximum draft values (denoted by the blue and green coding) tend to be associated with the darkest portions of the square law image which, as in the images of Figure 10 correspond to large floe-like areas of relatively flat ice. On the other hand, occurrences of larger (yellow, orange and magenta coding) maximum drafts tend to cluster in those portions of the monitored trajectory which traverse the concentrations of high brightness pixels which surround these flows. Close inspection, keeping in mind the positioning uncertainty (denoted by the added circle at the instrumented Chayvo site indicates that while bright image features are almost always present in the vicinity of large draft values, other bright image features are just as clearly detected along the track at distances from significant maximum draft values which are greater than the positioning uncertainties. As well, we found no consistent correlations between either the intensity or number of bright image points and the exact magnitudes of nearby large maximum draft values. The latter discrepancy is not unexpected, given that the small footprint of the IPS4 allows sampling of only a small fraction of a ridged ice feature while Radarsat imaging, in principle, returns data from all above-water portions of the same feature. Nevertheless, both our comparisons and prior experience (Melling, 1998) suggest that while Radarsat imaging does record exceptionally strong signal returns from large ridged ice features, one cannot simply and unambiguously either link the strengths and spatial extent of such returns to ridge height and extent or rule out the possibility that strong, spatially extensive returns may be associated with areas occupied by highly radar-reflective young ice or rough water.

Similar but somewhat more promising results were obtained with the April 1 fine beam image after application of a dissimilarity texture filter (Haralick, 1979). The portion of this image coincident with draft data acquired at the PA2 site is reproduced in Figure 12 along with a corresponding overlay of maximum keel drafts using the same colour-coding employed in Figure 11. It is evident that significant deep keels tend to be associated with large along-track gradients in the represented dissimilarity index (i.e. at the junctions of adjacent light and dark portions of the image). On the other hand, even this correspondence is not universal as can be seen in the uppermost portion of the ULS data track, where large dissimilarity gradients are associated with the actual edges of the imaged ice pack and show no coincident presence of deep ice keels.

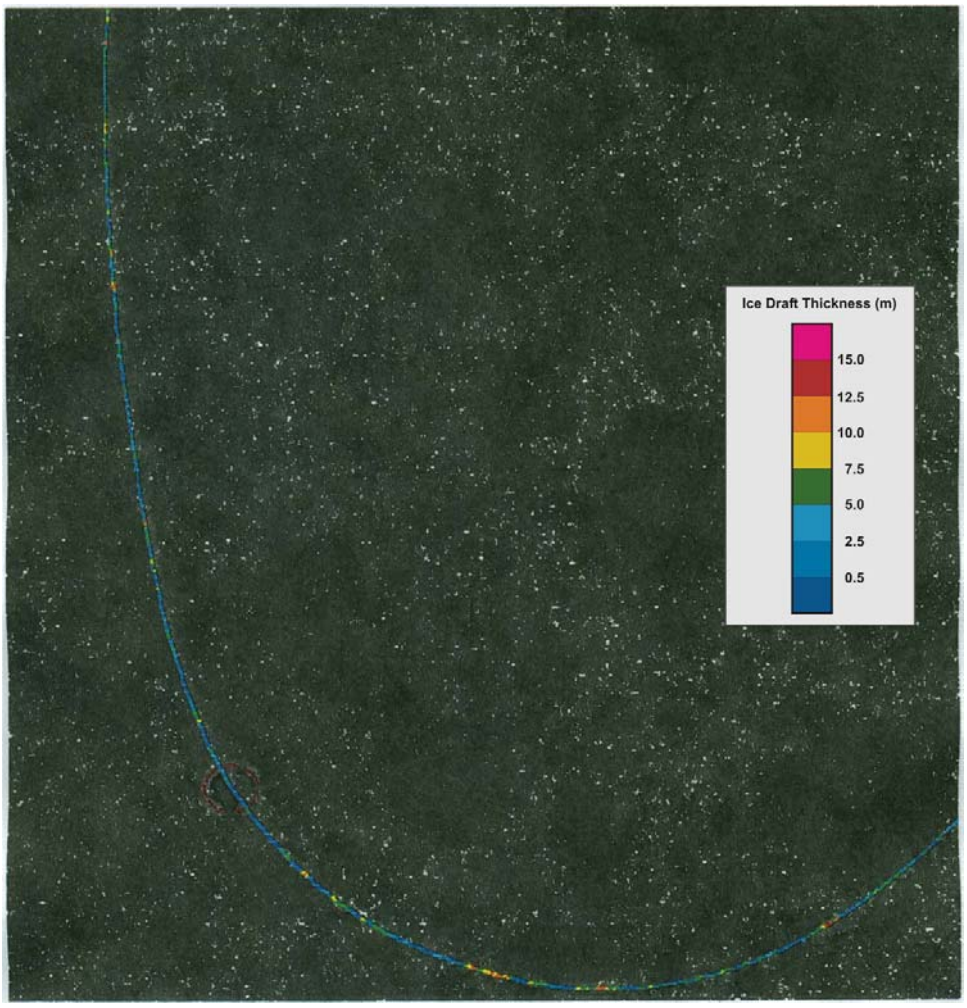

Figure 11. Colour-coded maximum draft data recorded at the Chayvo site superimposed upon the April 18, 1997 Fine Beam Radarsat image displayed with a square law grey-scale. The approximate positioning uncertainty is denoted by the open red circle.

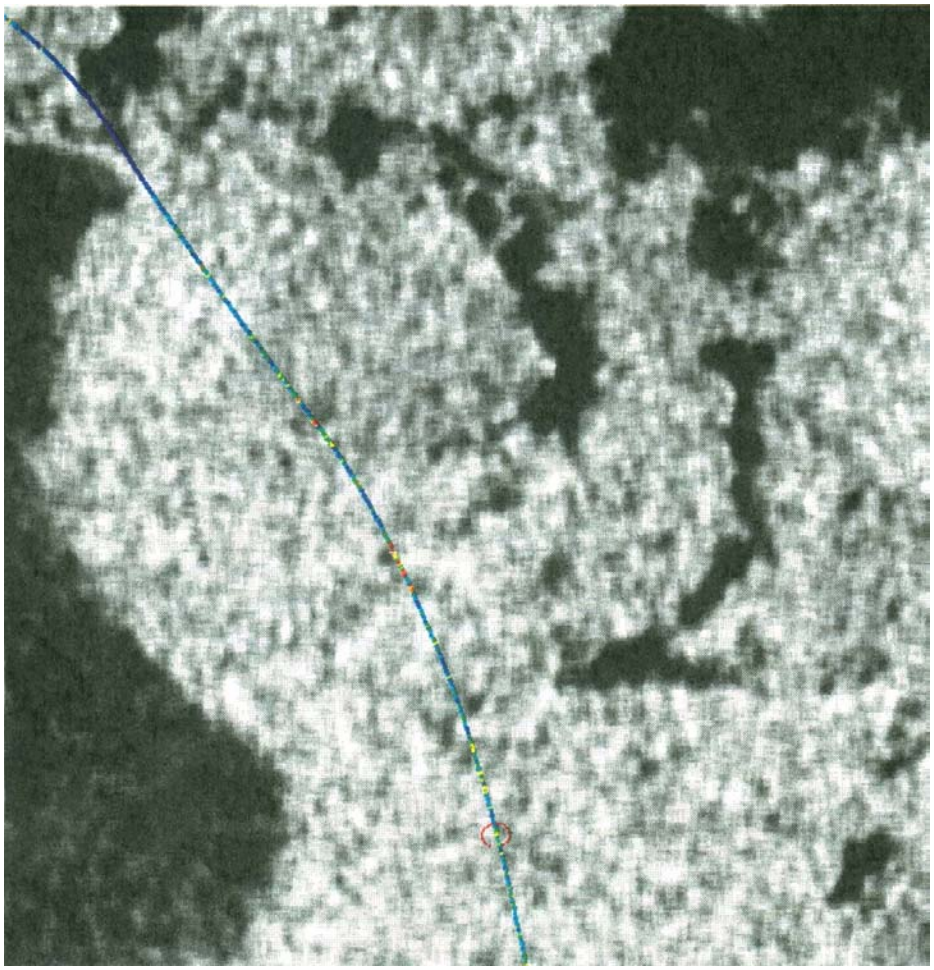

Figure 12. A portion of the April 1 Fine Beam Radarsat image of ice in the vicinity of the PA2 monitoring site (denoted by the uncertainty circle) after processing with a dissimilarity filter. The overlaid track if measured maximum draft data utilizes colour-coding identical to that employed in Figures 11.

CONCLUSIONS

The obtained results strongly suggest that, in spite of its steep viewing angles, Radarsat imaging does detect strong return signals from ridged sea ice. On the other hand, because of both the lack of a demonstrated firm linkage between the strengths and spatial extents of these signals, on the one hand, and ridge sail height (or keel depth), on the other, as well as frequent observations of equivalent signal returns from thin young ice and waves in open water, unambiguous ridge detection was not demonstrated in terms of simple signal strength indicators. Much more limited testing of texture-filtered images showed some promise in this regard but, again, the most effective detection strategy appeared to require an initial classification of the surveyed ice fields into ice type habitats with approximately known probabilities for hosting the large ridged ice masses of operational interest. Subsequently, in this approach, signal strength or texture signature detectors could be applied to high probability image portions. The initial classification step can be readily carried out for a given region through retrospective comparisons of Radarsat

imagery with coincidently acquired ULS draft data. In the present study, high probabilities for ridge occurrence were found to be associated with the "mottled" regions composed of distinct, relatively flat, floes embedded in a high reflectance ice matrix which was the most common host for deep ice keels. A second ice type, characterized by its distinctive radar image signature, was found to be of equivalent operational and technical interest because of its characteristic high values of roughness and mean thickness and its negligible content of deep keels. Offered speculations on the origins and mechanical properties of this ice type require additional study.

REFERENCES

Haralick, R.M. 1979. Statistical and structural approaches to texture. Proc. IEEE, **67**, pp. 786-804.

Marko, J.R., 2001.Large waves in thick interior Sakhalin pack ice. Proc. POAC '01. Ottawa, Canada, pp.233-242.

Marko, J.R., 2003. Observations and analyses of an intense waves-in-ice event in the interior of the Sea of Okhotsk ice pack. J. Geophys. Res.

Melling, H, 1998. Detection of features in first-year pack ice by synthetic aperture radar (SAR).Intl. J. of Remote Sensing, **19**, pp. 1223-1249.

Melling,H., P.H. Johnson and D.A. Reidel, 1995. Measurement of the draft and topography of sea ice by moored subsea sonar, J. Atmos. Oceanic Technol.**13**, pp.589-602.

Melling, H. and D.A. Reidel, 1996. Development of seasonal pack ice in the beaufort Sea during the winter of 1991-1992:A view from below. J. Geophys. Res.**101** , pp.11975-11991.

Pearson, D., C.E. Livingston, R.K Hawkins, A.L. Gray, L.D. Arsenault, T.L Wilkinson and K. Okamoto, 1980. Radar detection of sea-ice ridges and icebergs in frozen oceans at incidence angles from 0 to 90. In Proc. On Sixth Canadian Symposium on Remote Sensing, Halifax, Canada, pp. 231-237.

Wadhams, P. 1998. Sea Ice Morphology. In *Physics of Ice-Covered Seas* pub. Helsinki University Press, Helsinki, pp.231-288.